



### **Science Arts & Métiers (SAM)**

is an open access repository that collects the work of Arts et Métiers Institute of Technology researchers and makes it freely available over the web where possible.

This is an author-deposited version published in: <https://sam.ensam.eu>  
Handle ID: <http://hdl.handle.net/10985/22881>

#### **To cite this version :**

Wafa ELMAY, Laurent PELTIER, X. GABRION, Boris PIOTROWSKI, Pascal LAHEURTE, Sophie BERVEILLER, Regis KUBLER - Damping Capacity of Ti-Nb Shape Memory Alloys Evaluated Through DMA and Single-Impact Tests - Shape Memory and Superelasticity - 2022

Any correspondence concerning this service should be sent to the repository

Administrator : [scienceouverte@ensam.eu](mailto:scienceouverte@ensam.eu)



# Damping Capacity of Ti–Nb Shape Memory Alloys Evaluated Through DMA and Single-Impact Tests

W. Elmay<sup>1</sup> · L. Peltier<sup>1</sup> · X. Gabrion<sup>2</sup> · R. Kubler<sup>3</sup> · B. Piotrowski<sup>1</sup> · P. Laheurte<sup>4</sup> · S. Berveiller<sup>1</sup>

**Abstract** The present work deals with the study of the damping capacity of  $\beta$ -metastable Ti–(24–26) Nb alloys. In this work, several methods have been used to characterize this damping. The impact tests were carried out using two test benches: high-speed impacts were carried out using a vertical firing pressure gun and low-velocity impacts were studied with a bullet drop test. In addition, an original approach of a dynamic mechanical analysis (DMA) is proposed in order to obtain more in-depth understanding of the relationship between microstructure, deformation mechanisms, and damping capacity. The specimens are studied at different microstructure states: single  $\beta$ , dual-phase  $\beta + \alpha''$ , and martensitic phase. A correlation is established between the evolution of the damping factor as function of the applied strain and the occurrence of the

corresponding deformation mechanisms. The stress-induced martensite mechanism contributes to the improvement of the damping factor. The highest damping capacity is observed for the dual-phase specimen ( $\beta + \alpha''$ ). It is shown that the contribution of both the reorientation martensite variants and stress-induced martensitic transformation lead to a damping capacity higher than a single deformation mechanism one.

**Keywords** Titanium low-modulus alloys · Deformation mechanisms · DMA analysis · Single-impact test · Damping factor

## Introduction

Shape memory alloys are more and more used for damping applications: high-precision instruments, vibration and noise problems, protection of civil constructions as buildings and bridges [1, 2]. The energy dissipation capability for the shape memory alloys is mainly associated to the thermoelastic martensitic transformation [3]. In the literature, most of works concerning the investigation of damping capacity have been conducted on Nitinol alloy (Ni–Ti alloy with an equal atomic percentages of the two elements) by studying the effects of annealing conditions and aging treatment [4, 5], the effects of frequency and experiment temperature [6], and the effects of composition by varying the Ni content from 49.89 to 51.0 at.% [7]. Many authors have also investigated the influence of the Ni atoms substitution by a third element on Ni–Ti alloy such as Cu [8, 9], Fe [10], and Nb [11, 12]. However, only few studies have dealt with the damping capacity of  $\beta$  metastable Ti-based alloys [13–15].

---

This invited article is part of a special issue of *Shape Memory and Superelasticity* honoring Etienne Patoor for his contributions to the field of phase transforming materials and shape memory alloys. The special issue was organized by Dr. Fodil Meraghni, Ecole Nationale Supérieure d'Arts et Métiers (Arts et Métiers Institute of Technology), and Dr. Dimitris Lagoudas, Texas A&M University.

---

✉ S. Berveiller  
sophie.berveiller@ensam.eu

<sup>1</sup> LEM3 (UMR CNRS 7239), Arts et Métiers Institute of Technology, Université de Lorraine, CNRS, HESAM Université, 4 rue Augustin Fresnel, 57070 Metz, France

<sup>2</sup> Department of Applied Mechanics, University of Bourgogne Franche-Comté, FEMTO-ST Institute, CNRS/UFC/ENSMM/UTBM, 25000 Besançon, France

<sup>3</sup> MSMP, Arts et Métiers Institute of Technology, 2 Cours des Arts et Métiers, 13617 Aix-en-Provence, France

<sup>4</sup> LEM3 (UMR CNRS 7239), Université de Lorraine, Arts et Métiers Institute of Technology, CNRS, HESAM Université, 4 rue Augustin Fresnel, 57070 Metz, France

The commonly used technique to investigate the damping capacity is the dynamic mechanical analysis (DMA) with a thermal transformation cycling approach [13–17]. Two peaks are identified for  $\beta$  titanium alloys. A first well-defined peak accompanied by a decrease of the storage modulus is associated to the  $\beta$ - $\alpha''$  martensitic transformation. The second one is a broad peak which is observed at lower temperature and associated to the martensite variant reorientation mechanism [13, 14]. Through the investigation of the martensitic transformation and the damping behavior of Ti–25Ta–25Al (wt%) alloy using DMA in tensile mode, Bertrand et al. have highlighted the two sources of damping in this alloy which are the friction at austenite/martensite and martensite/martensite interfaces [14]. In that work, the damping properties of a Ti–26Nb (at.%) and a Ti–24Nb (at.%) alloys have been investigated by DMA and single-impact tests.

## Experimental Procedure

Both Ti–26Nb and Ti–24Nb (at.%) alloys were elaborated by the cold crucible levitation melting technique using ultra-pure raw materials: titanium (99.99%) and niobium (99.9%) were provided by GoodFellow. The ingots were then homogenized at 1223 K during 25.2 ks under pure argon atmosphere followed by water quenching. Solution treatment (ST) was then carried out at 1173 K for 3.6 ks under pure argon atmosphere followed by water quenching. The transformation temperatures were determined from direct measurement using DSC [18] or deduced from mechanical tests at different temperatures [19]. The transformation temperatures  $M_f$ ,  $M_s$ ,  $A_s$ , and  $A_f$  were found to be about 250 K, 265 K, 272 K, and 290 K, respectively, for the Ti–26 Nb alloy; it was austenitic at room temperature. They were measured around 340 K, 370 K, 380 K, 415 K, respectively, for Ti–24Nb alloy; it was martensitic at room temperature.

Single-impact tests were performed using two test benches shown in Fig. 1. High-speed impacts (15 and 65 m s<sup>-1</sup>) were performed using a vertical shooting pressure gun. The steel shot was propelled on a cubic sample (16 × 16 × 16 mm<sup>3</sup>). The exact impact velocity was measured by laser barriers at the exit of the gun as well as by a high-speed camera that was used also to measure the rebound velocity. Lower velocity impacts were investigated with a drop ball test: a 10-mm-diameter ball was falling inside a quartz tube (1 m height) and hitting a cylindrical sample (diameter 12 mm) of the tested alloy that is slid into a socket. A mechanical blocker allows

stopping the ball before a second bounce in order to avoid multiple impacts. The impact and rebound velocities were measured with a high-speed camera. For both experiments, conducted at room temperature, the impacted surfaces of the samples were prepared by automatic grinding and polishing with suspension diamond grit. Each test condition was repeated at least three times for repeatability. Nevertheless, it is worth mentioning that drop weight tests may bring about some discrepancies and in some extend variability due to the dynamic effects. To overcome this issue, the tests have been repeated 20 times for each developed alloy.

The coefficient of restitution,  $e$ , of the shot colliding the sample [20] was measured from the impact test. Johnson [21] gave an analytical expression for an inelastic impact of a sphere with the assumption of the dynamic mean contact pressure being equal to three times the yield strength  $\sigma_y$ :

$$e = \frac{\text{rebound velocity}}{\text{impact } v} = 3.8 \left( \frac{\sigma_y}{E^*} \right)^{\frac{1}{2}} \left( \frac{\frac{1}{2} m V_i^2}{\sigma_y R^3} \right)^{-1/8},$$

where  $m$  is the mass of the shot,  $R$  its radius, and  $E^* = \left( \frac{1-v_s^2}{E_s} + \frac{1-v_t^2}{E_t} \right)^{-1}$  the equivalent Young modulus between the shot ( $s$ ) and the target ( $t$ ). The microgeometry of the dent was measured using a confocal microscope; the diameter,  $2R_0$ , and the depth  $z_0$  were extracted from 3D measurement [22].

The approach commonly used for dynamic mechanical analysis (DMA) is a thermal transformation cycling under various applied stresses. In this work, we propose a different approach. The samples with dimensions of  $1.72 \times 0.63 \times 80$  mm<sup>3</sup> were subjected to a dynamic solicitation at constant temperatures and increasing stepwise the applied strain amplitude, in tensile mode using DMA Bose Electroforce 3200 and under nitrogen atmosphere. A 30-min holding at test temperature was performed to ensure a homogenous temperature in the sample. The dynamic solicitation was a sinusoidal deformation oscillation with ten oscillatory periods: the static strain was varied from 0.35 to 1.85% with a constant dynamic strain ( $\epsilon_{dy}$ ) of 0.15% and a frequency of about 1 Hz. The strain rate was approximately  $10^{-4}$  s<sup>-1</sup>. The strain was calculate by divided the displacement by the initial gauge length, the stress was calculated by divided the load by the initial cross section. The test temperatures were chosen to measure the damping capacity of the alloy in the austenitic and martensitic phases, as well as in the two-phase state. Each test has been repeated three times to account for repeatability.

## Results and Discussion

### Single-Impact Tests

First damping properties were characterized using single-impact tests. Impact and rebound kinetic energy of the shot ball were calculated from the corresponding velocity, for each test conditions. Figure 2a presents the loss of energy (impact energy minus the rebound one), which can also be interpreted as the absorbed energy by the materials, as a function of the impact energy. Due to its high shot diameter, the drop test corresponds to the highest impact energy despite the slowest shot velocity. At a first glance, all the alloys seem to follow the same law: the loss of energy does not seem to vary between the alloys. The pressure gun tests are aligned on a same line while the drop tests are slightly above this tendency. In Fig. 2b, the absorbed energy has been calculated relatively to the impact energy:

$$\frac{\Delta E}{E} = \frac{E_{\text{impact}} - E_{\text{rebound}}}{E_{\text{impact}}} \quad (1)$$

This representation emphasizes differences between both Ti–Nb alloys. In most cases, the relative absorbed energy is greater for the austenitic Ti–26Nb alloy than for the martensitic Ti–24Nb one. Only the drop test does not fulfill this observation as the opposite trend is observed. From the microgeometry, the impact diameter ( $2R_0$ ) was

measured relatively to the shot diameter ( $D$ ) (Fig. 3a–c); it was compared with the affected zone diameter ( $2R_{\text{aff}}$ ) that was estimated via optical micrographs (Fig. 3b, c). The dent diameter is slightly smaller in the Ti–26Nb alloy than in the Ti–24Nb at a given condition test; it increases with increasing impact velocity as expected, from 6% in the drop test up to 35% at  $65 \text{ m s}^{-1}$ . From optical micrographs, we can note that the martensitic transformation has occurred in a zone larger than the impact one; the affected volume is about twice the dent one. In the Ti–24Nb alloy, the mechanism is reorientation of martensite; the affected zone was of the same magnitude as the previous alloy except for the test with 1 mm shot at the lowest velocity. In that case, no effect was observed outside the dent. So, the absorbed energy is due to an extended inelastic mechanism in both materials.

Pressure gun tests and drop tests were compared using the restitution factor (Fig. 4); the Johnson’s law was plotted considering  $\sigma_y$  being equal to 100 MPa (dotted lines) which is near the transformation stress (120 MPa) or the reorientation one (100 MPa). A second value  $\sigma_y$  of 300 MPa (full lines) was considered; it corresponds to the yield strength of both alloys.

Pressure gun tests are well reproduced when plasticity is taken into account while drop tests are better fitted when only martensitic transformation or reorientation are considered. So, it can be expected that part of the absorbed

**Fig. 1** Experimental set-up. **a** Pressure gun; **b** drop ball test

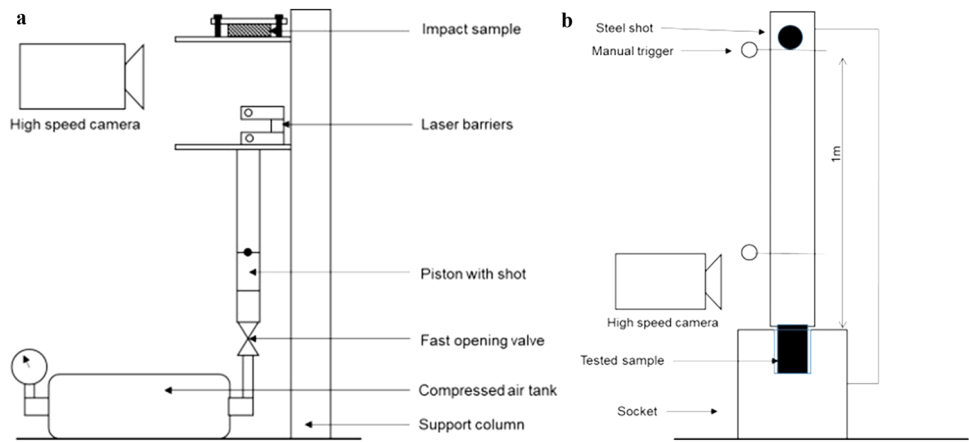


**Fig. 2** Absolute (**a**) and relative (**b**) absorbed energy (impact energy – rebound energy) as a function of impact energy

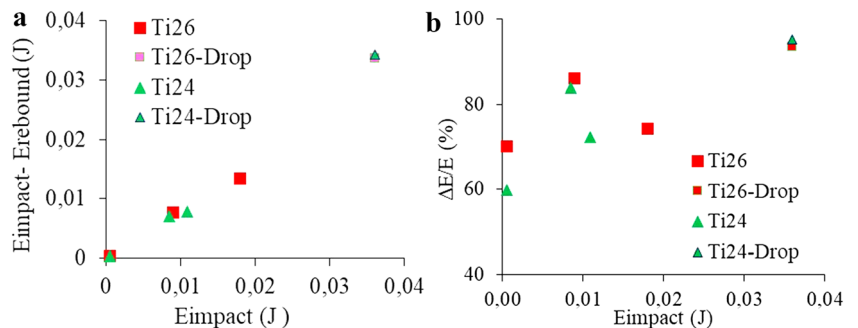


**Fig. 3** **a** Ratio of the dent diameter over the shot diameter as a function of the impact velocity. **b** Comparison of the affected zone radius ( $2R_{aff}$ ) and indent radius. **c** Impact micrographs of Ti-24Nb alloy (top) and Ti-26Nb alloy (bottom) as a function of shot diameter and impact speed

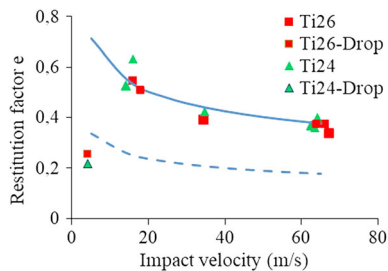
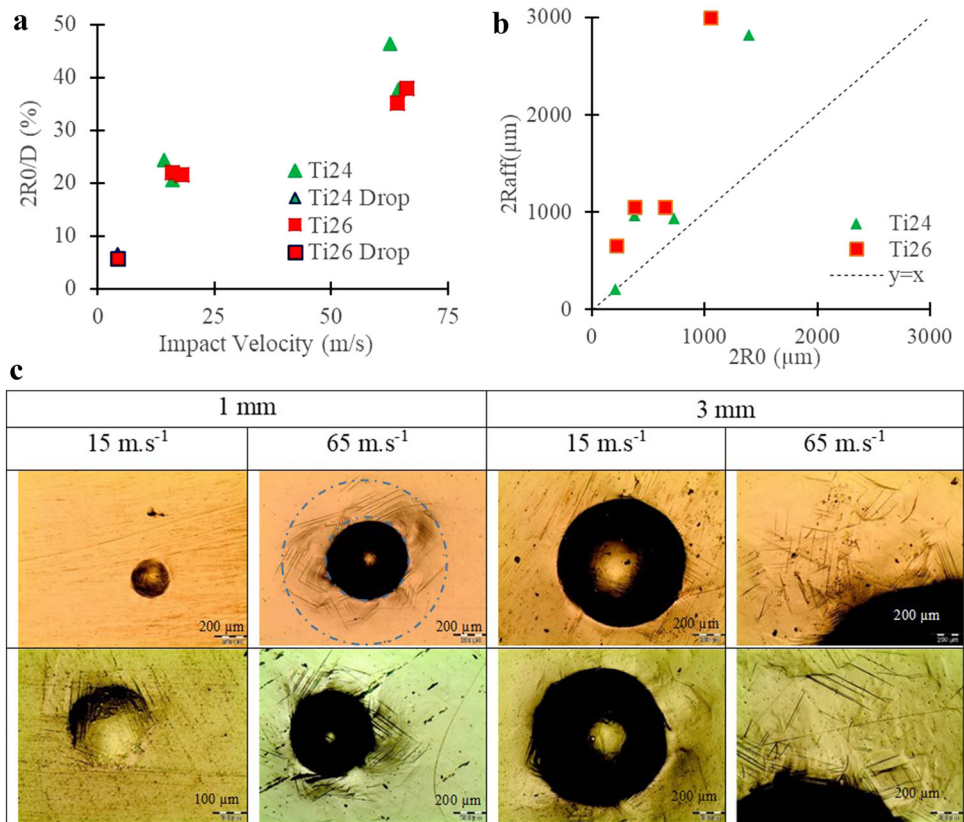


**Fig. 4** Restitution factor as a function of impact velocity for both alloys. Drop stands for drop test. Johnson law was calculated for a stress of 300 MPa (full line) and 100 MPa (dotted line)

energy has entailed plasticity by dislocations motion. In order to better characterize inelastic mechanism, samples were further analyzed by DMA; as the Ti-26Nb alloy has shown better results up to now, it was the only one tested by DMA.

## DMA

The samples were submitted to cyclic tensile loading at constant temperature, and for three different maximal strains (Fig. 5): at 298 K and 233 K, the alloy was, respectively, austenitic and martensitic, while both phases were co-existing at 258 K.

The evolution of the damping factor as a function of the imposed strain at different testing temperatures is shown Fig. 6.

We can note that the evolution of the damping factor depends on the temperature and the applied strain. The highest damping capacity (0.22) is observed at 258 K and 1% of the maximal applied strain while it is obtained at 233 K for higher strain level (1.5%). It is difficult to compare our damping factor values with the literature ones because of the difference in experiment protocol and the nature of alloys. Nevertheless, we can mention that the same order of magnitude was obtained with several studies using DMA analysis (Table 1) for titanium shape memory alloys [13, 23]. On the other hand, the values in this study are higher than that obtained for other categories of shape memory alloys such as Ni-Ti and Ni-Ti-C alloys [24], Cu-Al-Mn alloy [16], or in Ti50Ni38Cu(12-x)Nbx shape memory alloys (with  $x$  varying between 0 and 15%) [15].

Taking into account the specific evolution of the damping factor at different experiment temperatures, it is important to consider each case separately. At the temperature of 233 K (Martensitic state  $\alpha''$ ), the martensitic transformation is thermally induced which produces a self-accommodating growth of martensite with an equal probability for variants occurrence. In this configuration, the arrangement of the equiprobable variants on cluster

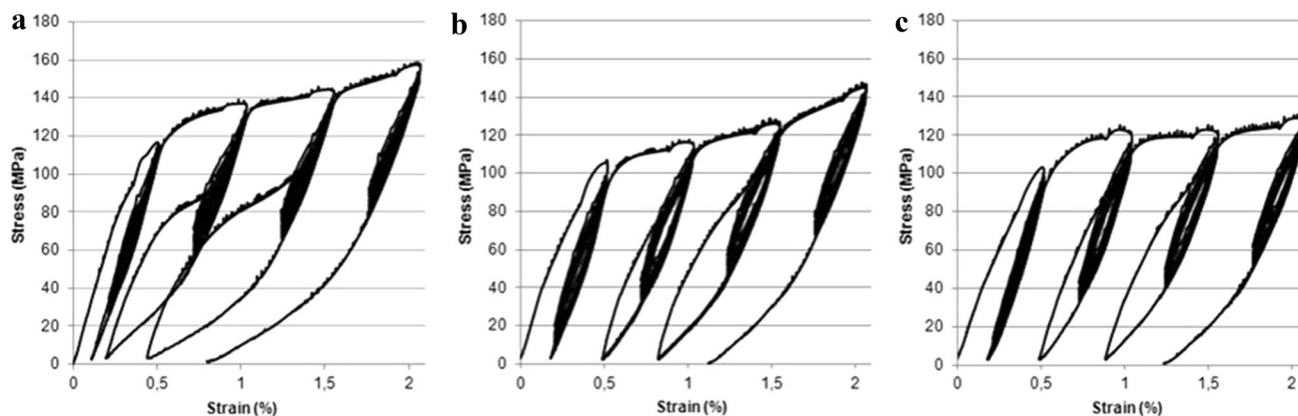


**Fig. 5** Strain–Stress curves under various temperatures obtained from DMA measurements on Ti–26Nb alloy: **a** at ambient temperature of 298 K, **b** at 258 K, and **c** at 233 K

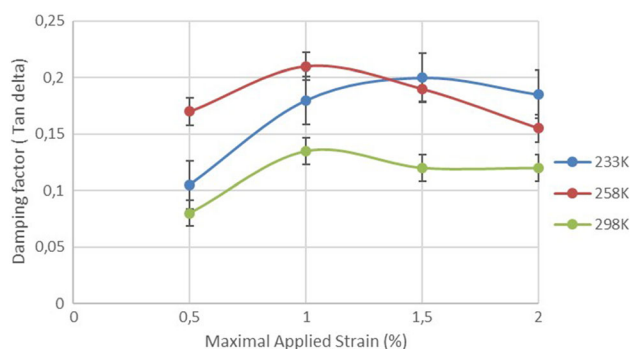


**Fig. 6** Evolution of damping factor as function of imposed strain at different testing temperatures for Ti–26Nb alloy

minimizes the total transformation shape strain. The feature of this self-accommodating microstructure has been studied for Ti–Nb alloys [13, 25]. It has been established that there are a particular twin relationships between the adjacent plates identified as the  $\{111\}\alpha''$  type I twinning or  $\langle 211 \rangle \alpha''$  type II twinning. The first imposed maximal strain level of 0.5% belongs to the elastic deformation domain for the martensitic structure inducing a low dissipation energy and consequently a low damping factor of about 0.11. Then, for higher strain level, the reorientation of variants occurs under stress plateau (Fig. 5c) with the growth of preferential variants which are favorably oriented to the detriment of the other variants [26]. The martensite variant is thus twinned into a preferential one by the motion of the twin boundary. So, under stress plateau, the motion of the twin boundaries at the martensite/martensite interfaces during the reorientation process leads to a high energy absorption which is at the origin of the high damping factor observed at 1% and 1.5% maximal strain level. The process of variants reorientation is reversible. However, at the end of the stress plateau, the reorientation variants mechanism is in an advanced state with the growth of favorably oriented variants.

At 298 K (austenitic state  $\beta$ ), the damping factor for the austenitic specimen is the lowest. This strain level corresponds to the elastic deformation domain of the austenitic phase. Then, the damping factor increases at 1% imposed strain to reach the value of 0.13 before a slight decrease and stagnation. The critical stress to induce martensitic transformation ( $\sigma_{SIM}$ ) of the  $\beta$  phase to the  $\alpha''$  phase is about 120 MPa (Fig. 5). At 1% maximal strain, since the stress level is higher than  $\sigma_{SIM}$ , the martensitic transformation mechanism occurs. This transformation and the movement of interfaces between austenite/stress-induced martensite interfaces contribute to energy dissipation leading to the increase of damping capacity at 1% strain. This martensitic transformation is reversible and it is at the origin of the superelastic effects. However, the repetitive phase changes of austenite/oriented martensite variants during cyclic solicitation introduce defects within the material. So, for higher imposed strain, these defects lead to the increase of the stress observed in Fig. 5, and therefore impeded partially the interface motion. At the intermediate temperature of 258 K (dual-phase state  $\beta + \alpha''$ ), the thermally induced martensitic transformation is partial, both  $\beta$  and  $\alpha''$  phases are present. The highest damping factor was obtained at 0.5% and 1% strain. For this dual-phase state, a large energy loss is due to the movement of both the interfaces of austenite/martensite variants and the martensite/martensite variants. It was reported that martensite variant reorientation and stress-induced martensitic transformation are possible to occur simultaneously at low stress levels due to the internal stress concentrations [27]. For higher strain level, a hardening is observed from the stress–strain curve (Fig. 5b) indicating that the strain is in part accommodated by plastic deformation mechanisms. This plastic deformation can induce an impediment to the movement of martensite/martensite and austenite/martensite interfaces leading to the

**Table 1** Damping factor of different SMA

Alloy	Damping factor	References
Ti–Nb–Al	0.15	[13]
Ti–24Nb–4Zr–8Sn	0.15–0.22	[23]
Ni–Ti and Ni–Ti–C	0.09	[24]
Cu–Al–Mn	0.078 and 0.14	[16]
Ti50Ni38Cu12xNb (with x Nb (0%,5%,10%, 15%))	0.168	[15]
Ti–26Nb	0.15–0.22	This work

consequent loss of damping capacity observed above 1.5% strain.

It can be deduced that the contribution of both martensitic transformation and reorientation variant lead to more energy dissipation than single deformation mechanism. Moreover, in dual phase, there are two types of martensite: self-accommodating martensite and stress-induced martensite. So, it allows concluding that the improvement of the damping capacity is related to the high number of martensite variants present within the specimen. This comment is in agreement with Chen et al. study which supports that the increase of the volume fraction of martensite contributes to the improvement of damping properties [24].

## Conclusion

The damping properties of Ti–Nb alloys were investigated via two single-impact tests and DMA. In the first tests, they were evaluated through the absorbed energy and the dent microgeometry after impact. As inelastic phenomena were also observed outside the dent, dimensions of the affected zone by such mechanisms were also measured and compared. The Ti–26Nb alloy in its austenitic state had the higher absorbed energy combined with the smallest dent radius; it means that the damping effect was mainly related to inelastic phenomena.

In a second time, an original approach of a dynamic mechanical analysis (DMA) was carried out to study the damping capacity of a  $\beta$ -metastable Ti–26Nb alloy. This approach consisted on applying a dynamic sinusoidal solicitation with a stepwise increasing applied strain. This protocol was driven at different constant temperatures wisely chosen to investigate the damping capacity under different microstructure states: single  $\beta$ , dual-phase  $\beta + \alpha''$ , and martensitic phase. It was shown in this study that the evolution of the damping capacity depends on the microstructure and on the deformation mechanisms activated under the different applied strain levels.

- the dual-phase specimen ( $\beta + \alpha''$ ) exhibits the highest damping capacity due to the occurrence of both

martensitic transformation and reorientation variant mechanisms. The high number of martensite variants (self-accommodating variants and stress-induced martensite) and consequently the high number of interfaces within this specimen is at the origin of the improvement of the damping capacity.

- the improvement of the damping capacity at 1% strain for the single  $\beta$  specimen is due to the dissipation energy occurring during the martensitic transformation.
- The martensitic specimen has the highest damping capacity under stress plateau corresponding to martensite variants reorientation. The motion of the twin boundaries at martensite/martensite interfaces leads to an important energy dissipation.

## Appendix

The applied strain  $\varepsilon(t)$  and the resultant stress  $\sigma(t)$  can be given by the following expressions:

$$\varepsilon(t) = \varepsilon_0 \sin(2\pi ft)$$

$$\sigma(t) = \sigma_0 \sin(2\pi ft + \delta),$$

where  $\varepsilon_0$  and  $\sigma_0$  are the strain and stress amplitudes, respectively;  $\omega = 2\pi f$  is the angular frequency and  $\delta$  is the loss angle by which the stress lags behind the applied strain.

These two quantities are related by a complex modulus  $E^*$  which is defined as follows:

$$E^* = E' + iE'' = \frac{\sigma^*}{\varepsilon^*} = \frac{\sigma_0}{\varepsilon_0} e^{i\delta},$$

where  $E' = \frac{\sigma_0}{\varepsilon_0} \cos \delta$  is the storage modulus and  $E'' = \frac{\sigma_0}{\varepsilon_0} \sin \delta$  is the loss modulus.

The ratio of these two moduli gives the damping factor:

$$\text{Tan} \delta = \frac{E''}{E'}$$

From our DMA measurement, the damping factor value is determined at each applied strain level, it represents the average of the phase lag obtained from the ten oscillatory periods.

## References

1. Song G, Ma N, Li H-N (2006) Applications of shape memory alloys in civil structures. *Eng Struct* 28:1266–1274
2. Van Humbeeck J (1999) Non-medical applications of shape memory alloys. *Mater Sci Eng A* 273–275:134–148
3. Humbeeck J (1996) Damping properties of shape memory alloys during phase transformation. *J Phys IV* 06(C8):371–380
4. Liu Y, Van Humbeeck J (1997) On the damping behaviour of NiTi shape memory alloy. *J Phys IV* 7(C5):519–524
5. Peltonen M, Lindroos T, Kallio M (2008) Effect of ageing on transformation kinetics and internal friction of Ni-rich Ni–Ti alloys. *J Alloy Compd* 460:237–245
6. Piedboeuf MC, Gauvin R (1998) Damping behaviour of shape memory alloys: strain amplitude, frequency and temperature effects. *J of Sound and Vib* 214:885–901
7. Yoshida I, Ono T, Asai M (2000) Internal friction of Ti–Ni alloys. *J Alloy Compd* 310:339–343
8. Yoshida I, Monma D, Iino K, Otsuka K, Asai M, Tsuzuki H (2003) Damping properties of  $Ti_{50}Ni_{50-x}Cu_x$  alloys utilizing martensitic transformation. *J Alloy Compd* 355:79–84
9. Li YH, Liu SW, Jiang HC, Wang Y, Deng ZY, Li YH, Wang CZ (2007) Analysis of the internal friction spectrum of TiNiCu alloy. *J Alloy Compd* 430:149–152
10. Yoshida I, Monma D, Ono T (2008) Damping characteristics of  $Ti_{50}Ni_{47}Fe_3$  alloy. *J Alloy Compd* 448:349–354
11. Cai W, Lu XL, Zhaon LC (2005) Damping behavior of TiNi-based shape memory alloys. *Mater Sci Eng A* 394:78–82
12. Chen Y, Jiang HC, Liu SW, Rong LJ, Zhao XQ (2009) The effect of Mo additions to high damping Ti–Ni–Nb shape memory alloys. *Mater Sci Eng A* 512:26–31
13. Inamura T, Yamamoto Y, Hosoda H, Kim HY, Miyazaki S (2010) Crystallographic orientation and stress-amplitude dependence of damping in the martensite phase in textured Ti–Nb–Al shape memory alloy. *Acta Mater* 58:2535–2544
14. Bertrand E, Castany P, Gloriant T (2013) Investigation of the martensitic transformation and the damping behavior of a superelastic Ti–Ta–Nb alloy. *Acta Mater* 61:511–518
15. Liu MY, Qi WY, Tong YX, Tian B, Chen F, Li L (2018) Study of martensitic transformation in TiNiCuNb shape memory alloys using dynamic mechanical analysis. *Vacuum* 155:358–360
16. Sutou Y, Omori T, Koeda N, Kainuma R, Ishida K (2006) Effects of grain size and texture on damping properties of Cu–Al–Mn-based shape memory alloys. *Mater Sci Eng A* 38–440:743–746
17. Liao X, Wang Y, Fan G, Liu E, Shang J, Yang S, Luo H, Song X, Ren X, Otsuka K (2017) High damping capacity of a Ni–Cu–Mn–Ga alloy in wide ambient-temperature range. *J Alloy Compd* 695:2400–2405
18. Peltier L, Berveiller S, Meraghni F et al (2021) Martensite transformation and superelasticity at high temperature of (TiHfZr)<sub>74</sub>(NbTa)<sub>26</sub> high-entropy shape memory alloy. *Shape Mem Superelasticity*. <https://doi.org/10.1007/s40830-021-00323-4>
19. Elmay W, Prima F, Gloriant T et al (2013) Effects of thermo-mechanical process on the microstructure and mechanical properties of a fully martensitic titanium-based biomedical alloy. *J Mech Behav Biomed Mater* 18:47–56
20. Fathallah R, Inglebert G, Castex L (2013) Determination of shot peening coefficient of restitution. *Surf Eng* 19:109–113. <https://doi.org/10.1179/026708403225002559>
21. Johnson KL (1985) Contact mechanics. Cambridge University Press, Cambridge
22. Guiheux R, Berveiller S, Kubler R, Bouscaud D, Patoor E, Puydt Q (2017) Martensitic transformation induced by single shot peening in a metastable austenitic stainless steel 301LN: experiments and numerical simulation. *J Mater Process Technol* 1(249):339–49
23. Yang Y, Castany P, Cornen M, Prima F, Li SJ, Hao YL, Gloriant T (2015) Characterization of the martensitic transformation in the superelastic Ti–24Nb–4Zr–8Sn alloy by in situ synchrotron X-ray diffraction and dynamic mechanical analysis. *Acta Mater* 88:25–33
24. Chen F, Tong YX, Lu XL, Wang X, Tian B, Li L, Zheng YF, Chung CY, Ma LW (2011) Effect of graphite addition on martensitic transformation and damping behavior of NiTi shape memory alloy. *Mater Letters* 65:1073–1075
25. Tobe H, Kim HY, Inamura T, Hosoda H, Nam TH, Miyazaki S (2013) Effect of Nb content on deformation behavior and shape memory properties of Ti–Nb alloys. *J Alloy Compd* 577:435–438
26. Elmay W, Berveiller S, Patoor E, Gloriant T, Prima F, Laheurte P (2017) Texture evolution of orthorhombic  $\alpha''$  titanium alloy investigated by in situ X-ray diffraction. *Mater Sci Eng A* 679:504–510
27. Liu Y, Xiang H (1998) Apparent modulus of elasticity of near-equiatomic NiTi. *J Alloy Compd* 270:154–159

**Publisher's Note** Springer Nature remains neutral with regard to jurisdictional claims in published maps and institutional affiliations.